12WCEE 2000

DISTANCE-DEPENDENT ATTENUATION FACTOR IN THE STOCHASTIC SIMULATION OF HIGH-FREQUENCY GROUND MOTIONS

Koshiro EN[1], Saori TAKAMI[2] And Arihide NOBATA[3]

SUMMARY

This paper discusses the quantitative estimation on high frequency contents of earthquake ground motion in the stochastic simulation method. The K-NET array data expanded in Kinki district in Japan is analysed to see the wave propagation properties. In the conventional formula, the distance attenuation is accounted for in the exponential form with the geometric spreading factor. The former term incorporates Q-value determined by the spectral inversion analysis given the shear wave velocity β. Here, the distance-dependency of β and Q is estimated for the different set of data considering the applicable scale of the field. Based on the estimated results for the apparent β and Q, the element waves are generated by the stochastic method following Boore(1983) in order to synthesise analytical waveform. Through the simulated results for the near-fault records around Kobe in Hyogo-ken Nambu Earthquake, the apparent smaller β and Q value in the near field implies rapid attenuation with increasing distance and frequency.

INTRODUCTION

Through the analysis on the observed records of Hyogo-ken Nambu Earthquake in 1995 (Mw=6.9), it has become clear that the data obtained near the fault does not show high frequency components as rich as expected by the conventional attenuation law. Even though the typical waveform of relatively long period of 1 to 2 second is explained by the effect of radiation pattern and directivity in the seismogenic region (e.g., Koketsu(1998)), it's not fully studied in the shorter period. This paper discusses the quantitative estimation on high frequency contents in the stochastic simulation method focusing on distance attenuation property.

The array data by K-NET (Kinoshita et al.(1997)) expanded in Kinki district in Japan is analysed to see the wave propagation properties. In the conventional formula, the attenuation through the heterogeneous path of wave trains is accounted for in the exponential form with the geometric spreading factor. The former term incorporates the unitless Q-value implying measure of physical absorption, which is determined by the spectral inversion analysis given the shear wave velocity β. Here, the distance-dependency of β and Q is estimated for the different set of data considering the applicable scale of the field. Based on the estimated results for the apparent β and Q, the element waves are generated following Boore(1983) in order to synthesise analytical waveform. Taking into account the distance-dependency of the attenuation factor, the stochastic simulation is presented to realise the near-fault records obtained around Kobe in Hyogo-ken Nambu Earthquake.

OBSERVED RECORDS BY K-NET

K-NET array organised by National Research Institute for Earth Science and Disaster Prevention, Science and Technology Agency, Japan, has presented reliable data of earthquake ground motion at 1000 sites in Japan in these several years. Among those data, we can get the records of intraplate earthquakes having their sources at the depth of 10 to 20 kilometres just under the sites in Kyoto. Such data are valuable in analysing the properties

[1] *Obayashi Corporation, 1-19-9 Tsutsumi-Dori, Sumida-ku, Tokyo, 131-8510 Japan Email : en@o-net.obayashi.co.jp*
[2] *Obayashi Corporation, 1-19-9 Tsutsumi-Dori, Sumida-ku, Tokyo, 131-8510 Japan*
[3] *Obayashi Corporation, 1-19-9 Tsutsumi-Dori, Sumida-ku, Tokyo, 131-8510 Japan*

of a city-attacking quake like Hyogo-ken Nambu Earthquake, which brought us significant damage. We use them with some of the interplate earthquakes to compare the wave propagation properties depending on the path of wave trains. Although JMA (Japan Meteorological Agency) magnitudes of the intraplate earthquakes detected in Kyoto are limited around 4, the knowledge on them should be useful in the wave synthesis of strong ground motion for larger events.

The principal parameters of the events studied are listed up in TABLE 1. The locations of their epicentres and the observatories are shown in Fig.1. We divide all the events into 2 groups, one of which, A, includes the intraplate earthquakes with their sources in rather shallow zone around Kyoto and the other, B, corresponds to the interplate earthquakes which occurred at the upper surface of Philippine Sea Plate. For each event, a listed number of sites present available data of three components (in 2 horizontal and 1 vertical directions).

The peak acceleration value of each record is plotted against the hypocentral distance in Fig.2 to see the inherent distance attenuation property. For the horizontal component, the mean value of NS (North-South) and EW (East-West) components is compared with the existing formula predicted by Fukushima and Tanaka (1991). Even though the data show large deviation, the average of them agrees with the prediction. The vertical component has similar property except that the absolute value is almost a half the horizontal component. For the data very near the source, for instance, in the range of the hypocentral distances less than 20 kilometres, the logarithm of the peak value keeps linear relation with that of the distance, and the maximum limitation is not observed. It seems to be partly because of relatively small magnitude of the events.

TABLE1 Principal parameters of the events studied.

Event No.	Date (m/d/yr.)	Depth (km)	Magnitude JMA(M)	Number of sites	Velocity β (km/s)
A-1	5/29/1996	17.0	3.9	9	3.42
A-2	7/18/1996	17.0	4.0	8	3.15
A-3	1/ 8/1997	13.0	4.0	12	3.46
A-4	9/ 7/1997	17.0	4.2	15	3.51
A-5	9/16/1997	18.0	3.8	11	3.33
A-6	2/12/1999	20.0	4.4	18	3.34
A-7	3/12/1999	20.0	4.1	12	3.34
B-1	6/ 9/1996	62.0	4.0	6	3.58
B-2	3/16/1997	39.0	5.8	19	3.76
B-3	5/24/1997	30.0	5.6	11	3.81

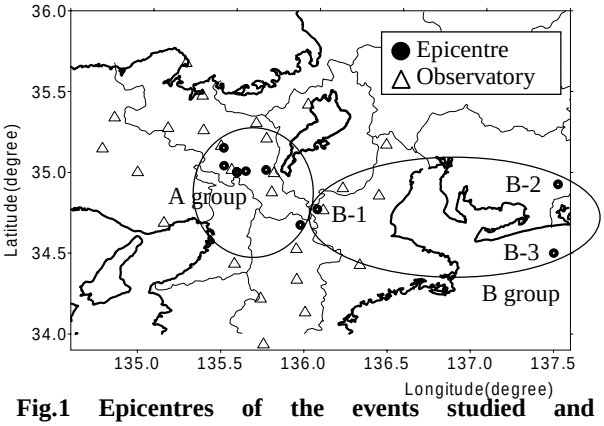

Fig.1 Epicentres of the events studied and observatories

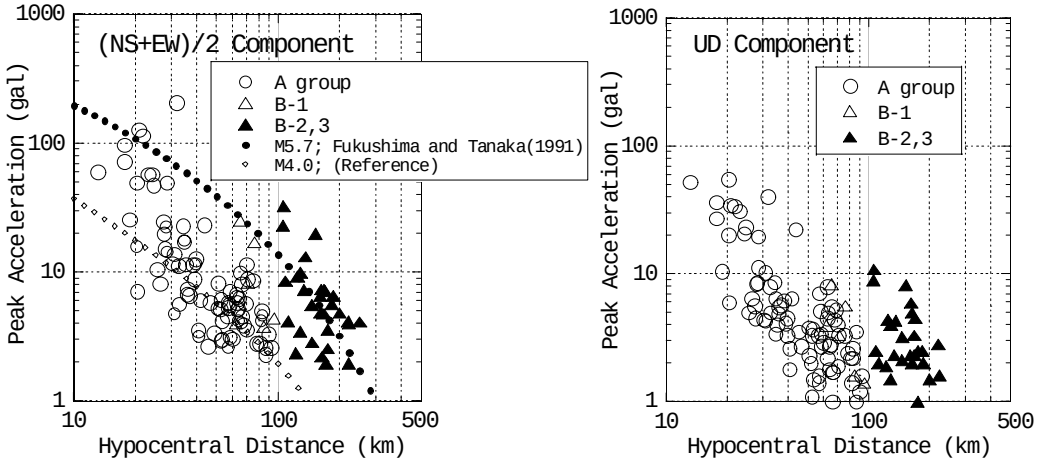

Fig.2 Distance Attenuation of peak acceleration value (left; horizontal, right; vertical component).

WAVE PROPAGATION AND DISTANCE ATTENUATION PROPERTIES

Wave Propagation Velocity

To obtain the wave propagation velocity, the arrival time of S (shear) wave is detected for each record 'by eye'. As shown in Fig.3, the S wave propagation time is computed to plot against the hypocentral distance for all the

data of each event. The regression analysis is carried out to determine the velocity that should represent the S wave "apparent average velocity" through the path from the source to the site. Of course, the thickness and the stiffness of the surface layer is different depending on each local site, thus, to be exact, we may need the correction for the estimated arrival time. However, we used it as it is, based on the judgement that there is not extreme difference in the soil conditions and the estimated error 'by eye' absorbs such deviation.

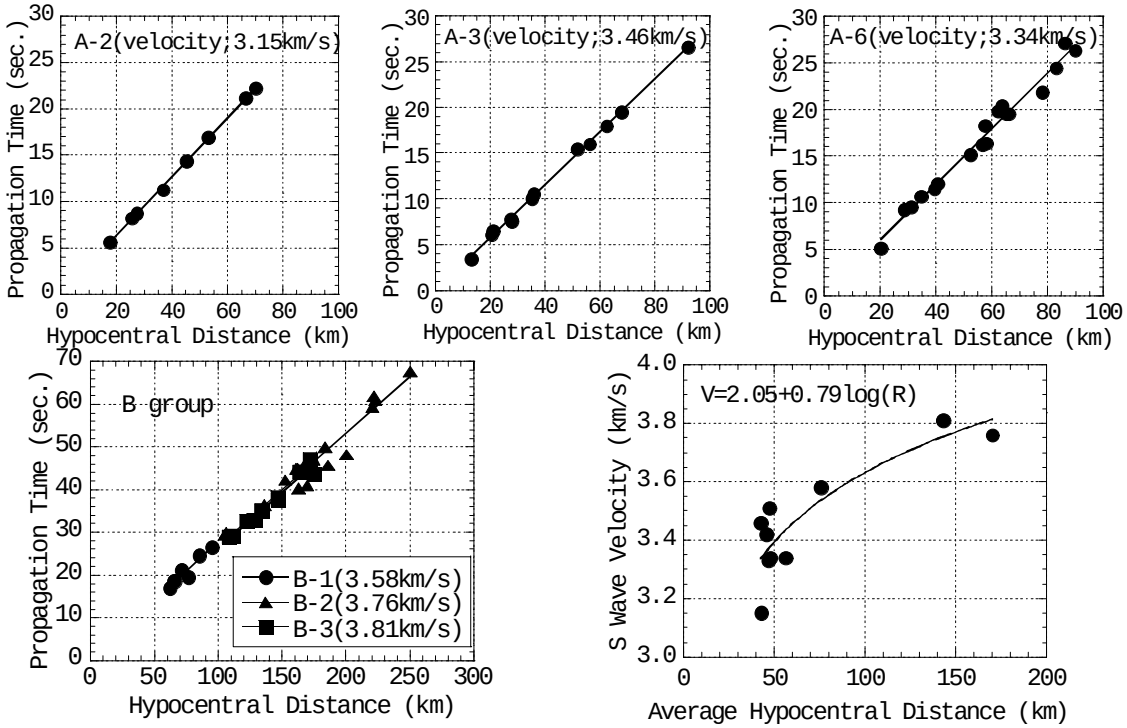

Fig.3 S wave velocity obtained by the regression analysis (upper; A group, lower; B group).

Fig.4 The relation of S wave velocity with the average hypocentral distance.

The results for all the events are shown in the right-side column of TABLE 1. The average value for each group is computed with the weights of the number of the observed sites; 3.38 km/sec. for A and 3.75 km/sec. for B. The difference in the velocity between both groups reflects the difference of wave-propagating path. It is noted that if the regression is applied for the epicentral distance instead of the hypocentral one, we'll get velocities of 3.7 to 3.9 km/sec. for the events of A and B. From the above results, the "apparent average velocity" explicitly includes the effect of the surface low-velocity layer more in the nearer-source event, while the seismic bedrock consists of a medium of rather stable velocity. To incorporate the distance-dependency of the attenuation factor in the wave propagation process, the "apparent average velocity" will be used. Fig.4 shows the relation of the S wave velocity with the average hyocentral distance, $\overline{R}$,as inferred in equation (1).

$$\beta(\overline{R}) = 2.05 + 0.79\log(\overline{R}) \tag{1}$$

Spectral Inversion Analysis

Through the spectral inversion analysis for the data obtained at multi-sites of some events, Q value of the "average path" is determined with the source spectrum for each event and the amplification factor at each site. By introducing the distance-dependent S wave velocity, $\beta(R)(\equiv \beta(R))$, the basic formula is as follows;

$$O_{ij}(f) = S_i(f)\cdot G_j(f)\cdot \exp\left(\frac{-\pi f R_{ij}}{Q(f)\beta(R_{ij})}\right)\frac{1}{R_{ij}}, \tag{2}$$

where $O_{ij}(f)$ is the Fourier amplitude spectrum of the observed record at the *j*-th site for the *i*-th event. It is expressed as the product of the source spectrum of the *i*-th event, $S_i(f)$, the attenuation factor of an exponential form including $Q(f)$, and the amplification factor at the *j*-th site, $G_j(f)$. R_{ij} is the hypocentral distance of the *i*-th event at the *j*-th site. Following Iwata and Irikura(1986), the least square method could be applied for each linear frequency, *f*. However, the original method requires the constraint condition in solving the problem, and

the solution cannot avoid the trade-off between $S_i(f)$ and $G_j(f)$. In this study, $Q(f)(=Q_{\bar{R}}(f))$ means the conditional Q value given the average distance of the applicable field. It is solved in the linear method by introducing the reference spectrum, $O_{iK}(f)$, at the fixed site, *K* (Moya et al.(1999)). By dividing both sides of equation (2) by $O_{iK}(f)$, we'll get

$$\frac{O_{ij}(f)}{O_{iK}(f)} = \frac{G_j(f)}{G_K(f)} \cdot \exp\left(\frac{\pi f R_{iK}}{Q(f)\beta(R_{iK})} - \frac{\pi f R_{ij}}{Q(f)\beta(R_{ij})} \right) \frac{R_{iK}}{R_{ij}} . \tag{3}$$

Taking the logarithm on both sides of equation (3), the equation with the unknown parameters, $Q(f), g_j(f)$, is derived as follows,

$$\log\left(r_{ij} \cdot o_{ij}(f)\right) = \log\left(g_j(f)\right) + (\log e) \cdot \pi f \left(\frac{R_{iK}}{\beta(R_{iK})} - \frac{R_{ij}}{\beta(R_{ij})} \right) \cdot \frac{1}{Q(f)}, \tag{4}$$

where, $r_{ij} = \frac{R_{ij}}{R_{iK}}$, $o_{ij}(f) = \frac{O_{ij}(f)}{O_{iK}(f)}$, $g_j(f) = \frac{G_j(f)}{G_K(f)}$.

To be noted is that the reference site, *K*, is selected to have the records for all the events. As predicted form the above equations, the stable solution is difficult to get from thin data set. Fig.5 compares $1/Q(f)$ obtained through the inversion analysis for the data of A and B group, respectively. The gradient of $1/Q(f)$ for A is explicitly smaller than that for B, which means higher damping in high frequency range. Such difference might be caused by the difference of wave-propagation path as well the result in the wave velocity. The data used in the inversion for A consists of 37 records, the hypocentral distances of which are less than 60 km (the average distance is 30 km), while for B, 36 records, from 60 to 250 km (average 150 km). In the case of more extended data for A, i.e., all the records of the distances ranging to 90 km, the gradient of $1/Q(f)$ gets closer to that for B.

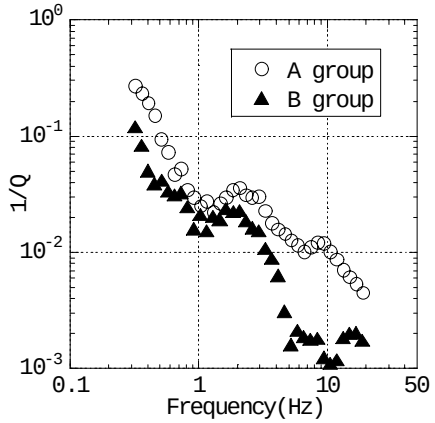

Fig.5 1/Q value obtained through spectral inversion analysis.

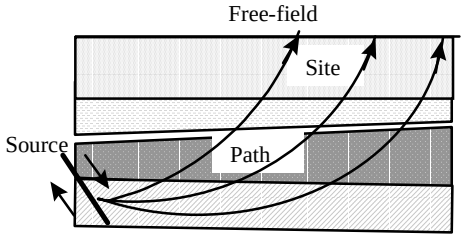

Fig.6 Schematic explanation in the difference of S wave velocity and Q value depending on the propagation path of wave trains.

Distance-Dependency of Attenuation Factor

Following Boore(1983), the acceleration Fourier spectrum at the free surface in the far-field is expressed in equation (5) under the assumption that the direct S wave is predominant.

$$A(f) = C \cdot \frac{M_0 (2\pi f)^2}{1 + (f/f_c)^2} \cdot P(f, f_{\max}) \frac{1}{R} \exp\left(\frac{-\pi f R}{Q\beta} \right). \tag{5}$$

In equation (5), M_0 is the seismic moment, f_c is the corner frequency, and $P(f, f_{\max})$ is a high-cut filter of a function of $f_{\max}$ defined as follows.

$$P(f, f_{\max}) = \frac{1}{1 + (f/f_{\max})^m} \qquad \text{(in our study, } m = 1\text{)}. \tag{6}$$

The coefficient *C* is given by equation (7), which includes the radiation pattern, $R_{\theta\phi}$ (=0.63 by Boore and Boatwright(1984)), the amplification due to the free surface, *FS* (herein after; =2), the reduction factor, *PRTITN*

(herein after; =0.71), accounting for the partitioning of energy into two horizontal components, and the geometric spreading factor.

$$C = \frac{R_{\theta\phi} \cdot FS \cdot PRTITN}{4\pi\rho\beta^3} . \qquad (7)$$

We set the density as $\rho = 3.0\,\mathrm{g/cm^3}$. The total attenuation with distance is contributed to by both factors of geometric spreading and anelastic attenuation of the exponential form. Now, we incorporate the distance-dependent attenuation property replacing β and Q by $\beta(R)$ and $Q_{\bar{R}}(f)$, respectively. As discussed in the previous section, those parameters reflect the characteristics of the path of wave trains as schematically shown in Fig.6. Assuming two Q models which have different coefficients of power to the frequency and substituting equation (1) into equations (5) and (7), we can see the effects of them on the distance-dependency of the acceleration Fourier amplitude spectra as shown in Fig.7.

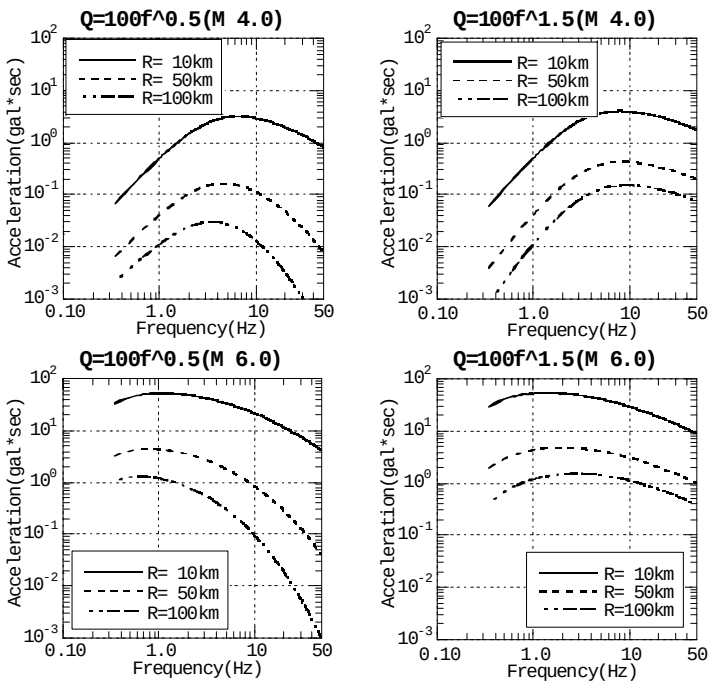

Fig.7 The effects of the distance-dependent shear wave velocity and the assumed Q value on acceleration Fourier spectra.

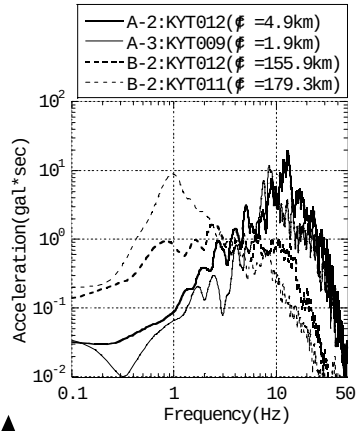

Fig.8 The observed spectra by K-NET for the typical cases of near and far-field events.

The estimated formula for $\beta(R)$ and $Q_{\bar{R}}(f)$ (Q is ideally modelled as a function of R ; $Q(R, f)$) need to be verified through the intensive work using more data. That is also the case for other parameters adopted in the following relations associated with the scaling law of the source properties;

$$\log M_0 = 1.5M + 16.2 \quad ; \text{Sato(1979),} \qquad (8)$$

$$f_c = 4.9\times10^6 \beta\left(\Delta\sigma / M_0\right)^{1/3} \quad ; \text{Brune(1970,1971), } \left(\Delta\sigma = 100\,(\text{bar})\right) \qquad (9)$$

$$f_{\max} = 7.31\times10^3 M_0^{-0.12} \quad ; \text{Faccioli(1986).} \qquad (10)$$

However, as illustrated in Fig.8, the observed data show similar properties in their spectral shape. The apparent smaller wave propagation velocity and smaller Q value for the near field event than those in the relatively far field event implies rapid attenuation with increasing distance and frequency.

STOCHASTIC SIMULATION OF STRONG MOTION NEAR THE FAULT

Boore's Element Waves

Stochastic waveform synthesis is proposed by Kamae et al.(1991) in predicting strong ground motion based on the scaling law of earthquakes. They generated the element waves following Boore(1983) to use them in the synthetic procedure accounting for the fault parameters. We apply this procedure to simulate the near-fault records around Kobe in Hyogo-ken Nambu Earthquake. Our interests are focused on the high-frequency contents observed less than expected in the near-fault region.

In Boore's method, a windowed time sequence of band-limited random white Gaussian noise is provided to simulate the stochastic nature of high-frequency contents. After adjusting its mean spectrum to fit the specified

one, a transient accelerogram is obtained by transforming back to the time domain. In our study, the same process is taken with the same window function as Boore's. Only the differences are the scaling parameters introduced above and the duration time. For the many records of aftershocks of Hyogo-ken Nambu Earthquake presented by CEORKA (Committee on Earthquake Observation and Research in the Kansai Area), the authors (En et al.(1998)) tried to separate the direct S wave part from the subsequent diffracted and/or surface waves through the wavelet transform-based conditional sampling method. Based on the estimated duration of inferred direct wave part, the following analyses take twice of T_d by Dobry et al. as the duration of a time window.

$$T_d = 10^{0.43M-1.83} \quad ; \text{Dobry et al.(1978).} \tag{11}$$

Fig.9 compares the spectra of the typical aftershock records at the sites of rock or firm soil conditions (KBU and CHY) with the computed given the corresponding magnitude and distance. The geometric relations of the sites with the epicentres are given in Fig.10. The spectra accounting for distance-dependent attenuation factor in terms of $\beta(R)$ and $Q(R, f)$, assuming equations (1) and (12), simulate the observed results better than those with the fixed β (=3.5km) and Q ($=110 f^{0.5}$; Akamatsu(1980)) do. To be noted is the definition of Q value. In this case, we do not incorporate the amplification factor at each site. Hence, the assumed Q value is relatively larger than that obtained through the spectral inversion analysis.

$$Q(R, f) = 110 f^{0.01R} \tag{12}$$

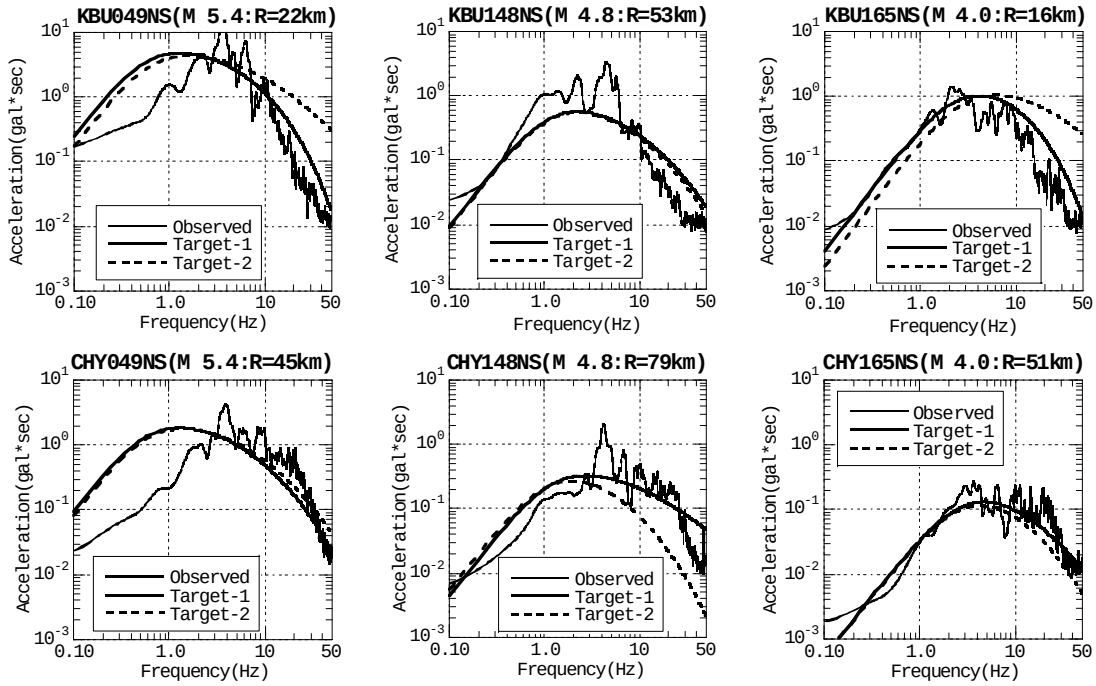

Fig.9 The comparison in the Fourier amplitude spectrum between the observed data and the specified targets based on Boore(1983)'s method. Taget-1 accounts for distance-dependent attenuation factor, while Taget-2 corresponds to the fixed shear wave velocity and Q value.

Waveform Synthesis of Strong Motion

In the waveform synthesis with a fault model, we need to specify the size and location of asperities and the quantitative evaluation of the stress drop. In this study, the source model by Kamae and Irikura(1998) is used, which is proposed by forward modelling through the empirical Green's function method. Their model consists of three asperities corresponding to three sub-events. The location and main parameters are shown in Fig.10. The element waves are assigned at the sub-area partitioning each asperity with the rupture velocity, 2.8km/sec. For each sub-event, a composite source model is applied with three sizes of element waves obeying power law to avoid the artificial period caused by the fault-division. The synthetic method is based on the improved version (Miyake et al.(1999)) of Irikura's(1986). The number of sub-areas is determined by the seismic moment-ratio between the synthetic and the element event. We define the minimum magnitude of element wave as 4.2.
By changing the seed of random generator for the phase properties, the stochastic simulation presents the fluctuation and variance in the waveform and spectrum of the synthesised result. We simulate 100 cases with the

unique condition except for the phase and estimate the average spectrum with its deviation. Fig.11 compares the simulated results with the observed for NS component at KBU, which is very close to the seismic fault, in pseudo velocity response spectrum for 5 per cent damping ratio. Although we do not take into account the amplification factor at the local soil, the direct comparison seems to be possible at the rock site. The simulated results can fairly explain the predominant period components of 1 to 2 second. In case that the fixed β and Q is used, however, high-frequency components are overestimated. Considering the distance-dependent attenuation factor, the simulated result is improved in the shorter period less than 0.2 second. It can explain the broadband frequency contents, qualitatively and quantitatively.

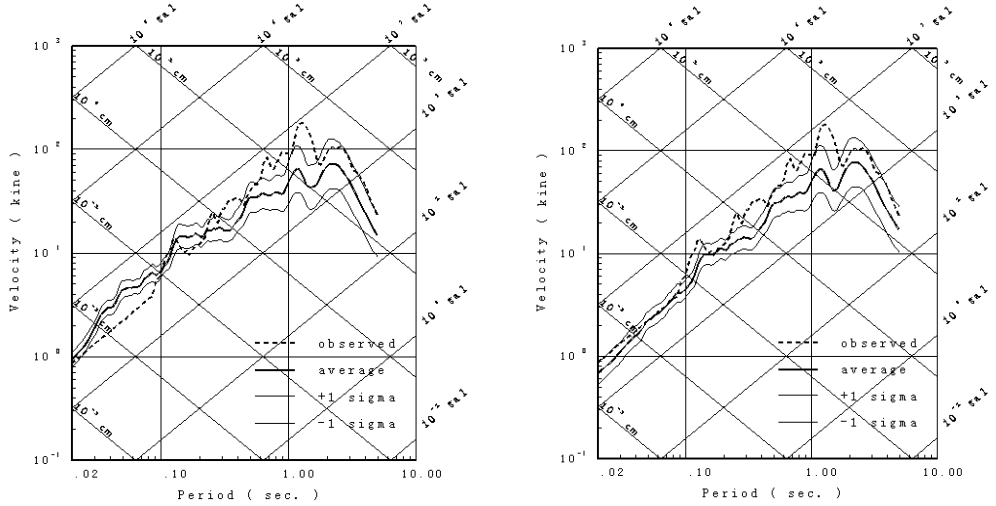

Fig.11 The comparison in pseudo velocity response spectrum between the observed data and the simulated for Hyogo-ken Nambu Earthquake in NS component at KBU. The left figure corresponds to the fixed S wave velocity and Q value, while the right accounts for distance-dependent attenuation factor. The result in stochastic simulation is expressed in terms of the average and its standard deviation.

CONCLUDING REMARKS

Through the work presented, the following lines have been identified as conclusions;

1) In the near field, the apparent wave propagation velocity and Q value is estimated smaller than those in the relatively far field, which implies rapid attenuation with increasing distance and frequency.
2) By accounting for the distance-dependent attenuation factor, it is possible to explain the reduced high frequency contents at the very close to the source.
3) The stochastic simulation method can explain the broadband frequency contents of the records observed at the site close to the seismic fault in Hyogo-ken Nambu Earthquake.

In our study, the distance-dependency of the wave propagation velocity and Q value is assumed based on the analyses on K-NET and CEORKA array data. The verification and the improvement of their estimation is recommended as a future work through the intensive analysis using more sufficient data.

ACKNOWLEDGEMENTS

We used the valuable data of K-NET by NRI for ESDP and the array by CEORKA, Japan. They stimulate us to do this research and are gratefully acknowledged.

REFERENCES

Akamatsu,J.(1980). Attenuation property of seismic waves and source characteristics of small earthquake. *Bull.Disas.Res.Inst.*, Kyoto Univ., 30, 53-80.

Boore,D.M.(1983). Stochastic simulation of high-frequency ground motions based on seismological models of the radiated spectra. *Bull.Seism.Soc.Am.*, 73, 1865-1894.

Boore,D.M. and J.Boatwright (1984). Average body-wave radiation coefficients. *Bull.Seism.Soc.Am.*, 74, 1615-1621.

Brune,J.N.(1970). Tectonic stress and the spectra of seismic shear waves from earthquakes. *J.Geophs.Res.*, 75, 4997-5009.

Brune,J.N.(1971). Correction. *J.Geophs.Res.*, 76, 5002.

Dobry,R., I.M.Idriss, and E.Ng (1978). Duration characteristics of horizontal components of strong-motion earthquake records. *Bull.Seism.Soc.Am.*, 68, 1487-1520.

En,K. and S.Takami (1998). Wavelet transform-based conditional sampling and spectral analysis on synthetic earthquake motion. *Proc.10th Jpn.Earthq.Eng.Symp.*, 1, 1181-1186 (in Japanese).

Faccioli,E.(1986). A study of strong motions from Italy and Yugoslavia in terms of gross source properties. *Geophs.Monograph*, 37, Maurice Ewing, AGU, 6, 297-309.

Fukushima,Y. and T.Tanaka (1991). A new attenuation relation for peak horizontal acceleration of strong earthquake ground motion in Japan. *Shimizu Tech.Res.Bull.*, 10, 1-11.

Irikura,K.(1986). Prediction of strong acceleration motions using empirical Green's function. *Proc.7th Jpn.Earthq.Eng.Symp.*, 151-156.

Iwata,T. and K.Irikura (1986). Separation of source, propagation and site effects from observed S-waves. *Zishin(J.Seism.Soc.Japan)*, 39, 579-593 (in Japanese).

Kamae,K. and K.Irikura (1998). Source model of the 1995 Hyogoken-Nanbu earthquake and simulation of near-source ground motion. *Bull.Seism.Soc.Am.*, 88, 400-412.

Kamae,K., K.Irikura, and Y.Fukuchi (1991). Prediction of strong ground motion based on scaling law of earthquake. *J.Struct.Constr.Engng, AIJ*, 430, 1-9 (in Japanese).

Kinoshita,S., M.Uehara, T.Tozawa, Y.Wada, and Y.Ogue (1997). Recording characteristics of the K-NET95 strong-motion seismograph. *Zishin(J.Seism.Soc.Japan)*, 49, 467-481 (in Japanese).

Koketsu,K.(1998). An overview of the rupture process. *Report on Hanshin-Awaji Earthquake Disaster, Common Series*, 2, 168-175, Maruzen, Tokyo (in Japanese).

Miyake,H., T.Iwata, and K.Irikura (1997). Strong ground motion simulation and source modeling of the Kagoshima-ken Hokuseibu Earthquake of March 26(M_{JMA}6.5) and May(M_{JMA}6.3), 1997, using empirical Green's function method. *Zishin(J.Seism.Soc.Japan)*, 51, 431-442 (in Japanese).

Sato,R.(1979). Theoretical basis on relationships between focal parameters and earthquake magnitude. *J.Phys.Earth*, 27, 353-372.